Silicon (2023) 15:1221–1233
https://doi.org/10.1007/s12633-022-02087-7

ORIGINAL PAPER

Comparative Characteristics of the Structure and Physicochemical Properties of Silica Synthesized by Pyrogenic and Fluoride Methods

Mirtemir Kurbanov[1] · Sardor Tulaganov[1] · Ulugbek Nuraliev[1] · Lyudmila Andriyko[2] · Olena Goncharuk[2,3] · Natalia Guzenko[2] · Yurii Nychyporuk[2] · Andrii Marynin[4]

Received: 13 July 2022 / Accepted: 31 August 2022 / Published online: 13 September 2022

Abstract
This paper presents the comparative analysis of the properties of highly dispersed silicas synthesized by pyrogenic and fluoride methods. Raw materials and synthesis conditions differ significantly for the considered methods. The structure and surface properties of synthesized silica samples was characterized by a number of methods such as IR, nitrogen adsorption, SEM, microcalorimetry, temperature programmed desorption time-of-flight with mass-spectrometry (TPDM), thermogravimetric analysis. IR spectra showed presence of characteristic absorption bending bands at 468 cm^{-1} (Si–O-Si) and at 800 cm^{-1} (O-Si–O) and stretching vibrations bands in the range of 1000–1200 cm^{-1} (Si–O-Si) for all the studied samples regardless of their synthesis method. The absorption band at 3750 cm^{-1} attributed to free silanol groups ≡Si–OH confirms the presence of this main sorption centers evenly distributed on the surface for all silica samples. The intensity of this band is quite low for samples obtained by the fluoride synthesis method due to the high water content. This fact is also confirmed by the TGA and TPDM methods. The distribution functions of the activation energy of water desorption demonstrates several maxima: (i) at 60–80 kJ/mol and 100 kJ/mol refers to desorption of molecularly adsorbed water; (ii) at 160–180 kJ/mol is due to the associatively desorbed water. All studied silica samples are hydrophilic according to values of the heat of immersion in water and n-decane, and their Rebinder's hydrophilicity index $K_h > 1$. The BET surface area and pore volume of samples significantly depend both on the method of synthesis and on the raw materials.

Keywords Fluoride method · Technogenic metallurgical waste · Synthesis · Properties of amorphous silica

1 Introduction

Silicon dioxide has been one of the objects of increased attention of researchers around the world for many years. A large number of scientific works have been devoted to the study of its structure and properties. The main research results are summarized in many monographs [1–8].

The most typical and stable silicon compound is SiO_2. This oxide has several crystalline modifications, among which the main ones are quartz, tridymite and cristobalite, which can transform into each other and each have α- and β-forms [3, 6].

A special place among the varieties of SiO_2 is occupied by amorphous highly dispersed silica (HDS), which the main industrial method of synthesis is the high-temperature hydrolysis of $SiCl_4$ in a hydrogen–oxygen flame [1, 3, 9], that can be described by the following general reaction (1):

$$SiCl_4 + 2H_2 + O_2 \overset{1200-1500^{\circ}C}{\rightarrow} SiO_2 + 4HCl \quad (1)$$

This method of HDS synthesis is known in the literature as a pyrogenic technology [2, 3, 6, 9].

Amorphous silica (SiO_2), in contrast to its crystalline form, has a developed surface [1–9]. Features of the surface

✉ Lyudmila Andriyko
andriykolyuda@gmail.com

[1] Institute of Ion-Plasma and Laser Technologies Named After U.A. Arifov, Durmon Yuli str., 33, Tashkent, Uzbekistan 100125

[2] Chuiko Institute of Surface Chemistry, NASU, 17 General Naumov Str., Kiev 03164, Ukraine

[3] National Technical University of Ukraine «Igor Sikorsky Kyiv Polytechnic Institute», Peremohy Avenue, 37, Kiev 03056, Ukraine

[4] National University of Food Technology, 68 Volodymyrska Street, Kiev 01033, Ukraine

structure and physicochemical properties make SiO_2 a good sorbent widely used in medicine [1] and in various industries [10, 11]. So, unmodified silicas can be directly used as fillers in the production of rubber, plastics, liquid thickeners and in other industries. [5, 7, 9, 12].

The surface properties of the dispersed amorphous SiO_2 (hydroxyl coating, active surface centers), developed specific surface, pore volume, density, strength, etc. play a decisive role in the interaction with polar and non-polar media, various substances and largely depend on the chemical composition, properties of the raw material used, as well as the conditions and technology of synthesis [13–15].

Due to the wide range of HDS applications, research on the development of new resource- and energy-efficient technologies for the SiO_2 synthesis is of great interest both to researchers and consumers of this product. At the same time, special attention is paid to technologies that do not require the usage of special raw materials and many reagents. For these purposes, metallurgical industrial wastes in the form of slags and microsilica from the copper and silicon-ferrosilicon production, respectively, can be used [16, 17]. It is shown that dispersed powders of amorphous silica with high purity and a relatively small S_{BET} in the range 60–65 m^2/g can be synthesized from such waste products by the fluoride synthesis method using a single reagent – ammonium fluoride (NH_4F) at temperatures not exceeding 400 °C according to the following reactions (2–3) [18, 19]:

$$SiO_2 + 6NH_4F \overset{200^\circ C}{\rightarrow} (NH_4)_2SiF_6 + 4NH_3 + 2H_2O \quad (2)$$

$$(NH_4)_2SiF_6 + 4NH_4OH \overset{320-400^\circ C}{\rightarrow} SiO_2 + 6NH_4F + 2H_2O \quad (3)$$

This approach meets the requirements of resource- and energy-efficient technologies, and also contributes to the solution of environmental problems associated with the production activities of metallurgical plants.

Thus, the aim of the study was to investigate the properties of the amorphous silicas, synthesized from metallurgical waste using the fluoride method as well as to analyze and identify their features in comparison with A-60 silica obtained by the pyrogenic synthesis method. To achieve this purpose, we used a number of amorphous silicas samples that differ significantly both in the raw materials and in the synthesis conditions. This approach would reveal the effectiveness of the application of non-traditional methods of synthesis and at the same time using non-standard and cheap raw materials, including technogenic metallurgical wastes. Such approach may also serve as a solution to some problems associated with environmental pollution.

2 Materials and Methods

2.1 Materials

Non-porous fumed silica A-60 ($S_{BET} = 80$ m^2/g, Pilot plant of Chuiko Institute of Surface Chemistry, Kalush, Ukraine) and highly dispersed SiO_2 powders synthesized from slag from the copper-smelting production of the Almalyk Mining and Metallurgical Combine (AMMC) (Si_{Slag}, Table 1) and microsilica (MS), which is dusty wastes from the production of ferrosilicon FeSi65 of Uzmetkombinat JSC (Si_{MS}, Table 1).

2.2 Synthesis

For the synthesis of amorphous SiO_2 from the slag and microsilica, a special device with a nickel alloy reactor was developed. A stainless steel condenser was used to separate and collect volatile products. The absorption of gaseous ammonia was carried out in a vessel with water, and the regeneration of NH_4F (or NH_4HF_2) was carried out in an evaporator. Fluorination of slags or microsilica was performed at temperatures up to 200 °C until powdered pitch was formed. Then the resulting mixtures of ammonium fluorine silicon compounds were processed at temperatures of 320–400 °C until the sublimation separation of ammonium hexafluorosilicate ($(NH_4)_2SiF_6$) according to reaction (2). After $(NH_4)_2SiF_6$ hydrolysis in an ammonia solution according to reaction (3) and filtration of the ammonia solution, SiO_2 powders were obtained, which were dried for three hours at 120–130 °C to obtain the final product marked as Si_{Slag} and Si_{MS} (Table 1). The synthesis technology is detailed in [18, 19].

Table 1 Raw materials, synthesis method and purity of silica samples

N	Synthesis method	Sample	SiO_2 purity, %	Raw materials
1	Pyrogenic *reaction (1)*	A-60	99.80	$SiCl_4$
2	Fluoride, *reaction (2,3)*	Si_{Slag}	99.96	Slags from the copper-smelting production of the AMMC
3	Fluoride, *reaction (2,3)*	Si_{MS}	99.86	Microsilica, which is dusty wastes from the production of FeSi65 of Uzmetkombinat JSC

2.3 Methods

2.3.1 Textural Characteristics

The low-temperature (77.4 K) nitrogen adsorption–desorption isotherms for all synthesized silica samples were recorded on a Kelvin-1042 adsorption analyzer (Costech Microanalytical). The samples were degassed at 110 °C for two h in a vacuum chamber. The values of the specific surface area (S_{BET}) were calculated consistent with the the standard BET method [20]. The total pore volume V_p was evaluated from the nitrogen ad-sorption at $p/p_0 \approx 0.98$–0.99, where p and p_0 denote the equilibrium and saturation pressure of nitrogen at 77.4 K, respectively [21]. The nitrogen desorption data were accustomed compute the pore size distributions (PSD_S, differential $f_V \sim dV_p/dR$ and $f_S \sim dS/dR$) using a self-consistent regularization (SCR) procedure under non-negativity condition at a parameter of regularization $\alpha = 0.01$ [22]. The differential PSD_S with relation to pore volume $f_V \sim dV/dR, f_V dR \sim V_p$ were re-calculated to incremental PSD (IPSD) at $\Phi_V(R_i) = (f_V(R_{i+1}) + f_V(R_i))(R_{i+1} - R_i)/2$ at $\sum \Phi_V(R_i) = V_p$). To calculate contributions of micropores (V_{micro} and S_{micro} at $0.35\ nm < R < 1\ nm$), mesopores (V_{meso} and S_{meso} at $1\ nm < R < 25\ nm$), and macropores (V_{macro} and S_{macro} at $25\ nm < R < 100\ nm$) the f_V and f_S functions were also used.

2.3.2 SEM

Microscopic images were recorded using Tescan Mira3 LMU scanning electron microscope, each image contains information about the shooting mode (SEM HV – accelerating voltage, usually was 10 kV, magnification (kx – 1000 times). All samples were spread with a thin film of palladium and gold.

2.3.3 Infrared Spectra

The transmittance infrared (IR) spectra were recorded using a Specord M80 (Carl Zeiss, Germany) in the range of 4000–400 cm^{-1} and converted to absorbance. The samples of initial silicas were pressed into thin pellets with size 8 ± 28 mm and mass 20 ± 0.5 mg and their mixture with KBr (Sigma-Aldrich, for spectroscopy) as 1:100, stirred and pressed into thin pellets with size 5 ± 20 mm.

2.3.4 Thermal Analysis

Thermal analysis (thermogravimetry, TG, differential TG, DTG) these samples were carried out in air using a Q-1500D derivatograph (Hungary) apparatus with computer data recording. Thermogram registration parameters for samples: A-60 – 303.0 mg, Si_{Slag} – 227.3 mg, Si_{MS} – 293 mg, sensitivity – 20 mg, TG-500, DTG-500, DTA-250 at a heating rate of 10 °C min^{-1} in the temperature range of 25–1000 °C.

2.3.5 TPD MS

Thermal desorption mass spectra (TPDMS) were studied using one-pass (OP) temperature programmed desorption (TPD) time-of-flight (ToF) method with mass-spectrometry control using a MSC-3 (''Electron", Sumy, Ukraine) ToF mass-spectrometer [23]. Pressure in a chamber was 4×10^{-6} Pa, sample weight was 7 mg (with a short distance (~0.5 cm) between a sample and a MS detector), and a heating rate (β) was 1.2 K/s. The sample was heated to a maximum temperature of 600 °C in 75 min linearly in time at a rate of 0.15 °C/s. At the same time, with the heating of the sample, the mass spectra were recorded on a computer, from which data on the time variation of the amplitude of the required components were then extracted and the dependences $I_m(t)$ were plotted.

The distribution function of the water desorption activation energy *f(E)* was calculated using the integral equation for one TPD peak

$$A(T) = \frac{c_1 T[\Theta(T)]^n}{\sqrt{2\pi\sigma^2}} \exp\left(-\frac{(T - T_m)^2}{2\sigma^2}\right) \int_{E_{min}}^{E_{max}} f(E) \exp\left(-\frac{E}{R_g T}\right) dE \quad (4)$$

where c_1 – constant, σ – the half-width of the desorption peak, T_m – the temperature of the water desorption maximum, $\Theta(T)$ – dependence of the surface coverage of hydroxyl groups on temperature, n – the reaction order ($n = 1$ for molecularly adsorbed and desorbed water, and $n = 2$ for associatively desorbed water), E_{min} and E_{max} – minimum and maximum value of activation energy (E) during integration. The equation can be solved using the regularization procedure, assuming that the normalized desorption and surface coverage of hydroxyl groups Θ(T) satisfy the condition [24, 25].

$$\int_{T_{min}}^{T_{max}} [\![\frac{A(T)}{\int A(T')dT'} + \Theta(T)]\!] dT = 1 \quad (5)$$

2.3.6 Microcalorimetry

The study of heats of immersion of highly dispersed oxides in water and *n*-decane carried out using a DAK-1 differential automatic calorimeter. The thermal effect of the process was measured with an accuracy of ± 1 μW at room temperature. Before measurements, the samples (50 mg) were placed in special ampoules and evacuated at 393 K and a pressure of

0.01 Pa for 2 h. After that, the ampoules were sealed off. The hermetic ampoules placed in a container with a liquid (distilled water, *n*-decane, 2 ml) in the calorimeter. The heat of immersion (Q) was calculated from the ratio:

$$Q = \frac{q}{m}, \tag{6}$$

where q – thermal effect of the process and m – mass of the evacuated sample in the ampoule.

The hydrophilicity index (K_h) was calculated as the ratio of the heat of wetting by the polar liquid (water) to the heat of wetting by the non-polar liquid decane [26]:

$$K_h = Q_w/Q_d. \tag{7}$$

3 Results and Discussion

3.1 Textural Characterization

The nitrogen adsorption isotherm for the obtained silicon dioxide sample is *S*-shaped. This isotherm shape points the occurrence of polymolecular adsorption. A curved initial section indicates a strong interaction of the adsorbate with the silica surface. At high pressures, the isotherm has a bend with a hysteresis loop (type IV) corresponding to the textural porosity of aggregates of nonporous nanoparticles (Fig. 1). The hysteresis loop shape indicates dominant contribution of mesopores predominantly cylindrical shape (filled by adsorbed nitrogen during the measurements) [20–22].

The textural characteristics of A-60, Si_{Slag} and Si_{MS} samples calculated from the nitrogen adsorption isotherms (Fig. 1a) are given in Fig. 1b and Table 2. The S_{BET} and pore volume of silica samples significantly depend both on the method of synthesis and on the raw materials. According to the low-temperature nitrogen adsorption data the SiO_2 samples have a S_{BET} about 80 m^2/g for A-60, 64 m^2/g for Si_{Slag} and the smallest value 11 m^2/g for Si_{MS}. All silica samples demonstrate pore size distributions with a predominant contribution from mesopores (Table 2, Fig. 1b). The mesopores area is 45 and 55 m^2/g for A-60 and Si_{Slag}, respectively. The minimal V_{meso} value 0.1 m^2/g is observed for Si_{MS}. But this sample has macropores area 10.2 m^2/g which is apparently related to the largest size of its particles and resulted in ineffective adsorption of nitrogen in macropores because the interactions of nitrogen molecules with large distant particles are very weak. The maximal values of total pore volume (V_p) of 0.218 cm^3/g and mesopore volume of 0.216 cm^3/g are inherent for sample Si_{Slag}.

The incremental pore size distribution (IPDS) functions (Fig. 1b) confirm the conclusion based on the isotherm shapes (Fig. 1a) that the silica samples are mainly

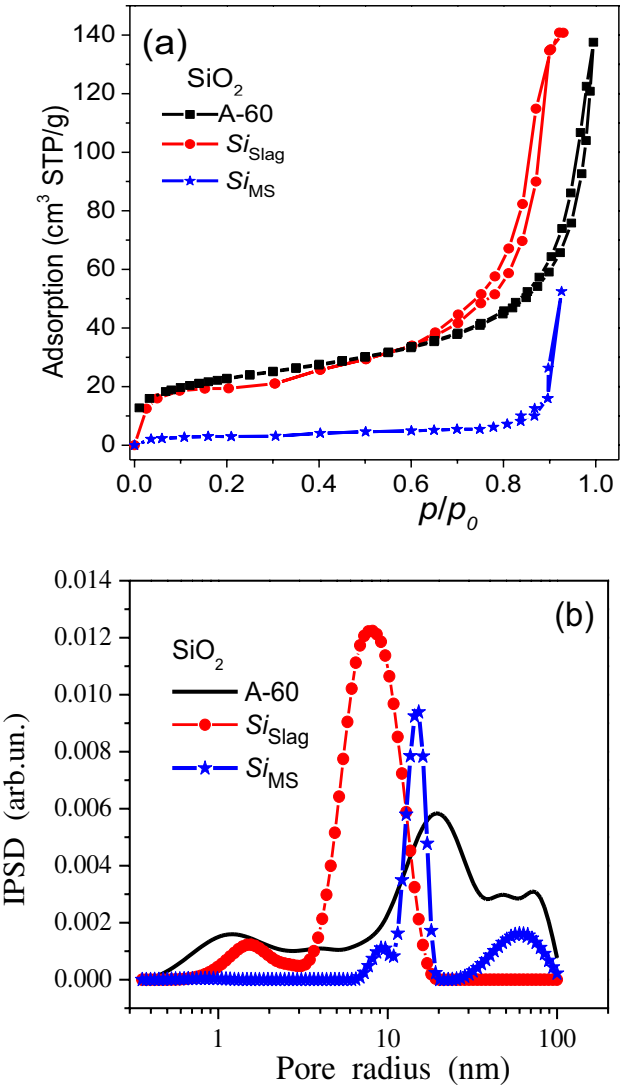

Fig. 1 Nitrogen adsorption–desorption isotherms (**a**) and incremental pore size distributions (**b**) for samples A-60, Si_{Slag} and Si_{MS}

mesoporous, since contributions of micropores and macropores are small (Table 2). Narrow voids between particles closely located in the same aggregates can also contribute to the porosity of the tested sample. Broader voids can be between distant non-porous nanoparticles in the same aggregate or neighboring aggregates [23, 27].

It is known that HDS powders are characterized by a certain structural hierarchy since primary nanoparticles form aggregates (50–1000 nm in size) and agglomerates of aggregates (> 1 μm) [13, 22, 25]. According to SEM data (Fig. 2), it can be seen that all studied silica samples have aggregated structures. Moreover, the Si_{Slag} sample is characterized by the predominant formation of particles in the form of flakes, on the surface of which small germ particles are fixed. These flakes, as well as particles of a more regular spherical shape, generate large agglomerates (Fig. 2a–c). For the Si_{MS} sample

Table 2 Textural characteristics of A-60, Si_{Slag}, Si_{MS} samples

Sample	S_{BET}, m^2/g	S_{micro}, m^2/g	S_{meso}, m^2/g	S_{macro}, m^2/g	V_{micro}, cm^3/g	V_{meso}, cm^3/g	V_{macro}, cm^3/g	$V_{p,}$ cm^3/g	$R_{p,V}$ nm
A-60	80	32	45	3.2	0.014	0.13	0.07	0.21	23.8
Si_{Slag}	64	8.5	55	0	0.002	0.22	0	0.22	7.6
Si_{MS}	11	0.2	0.1	10.2	0	0.06	0.02	0.08	25.6

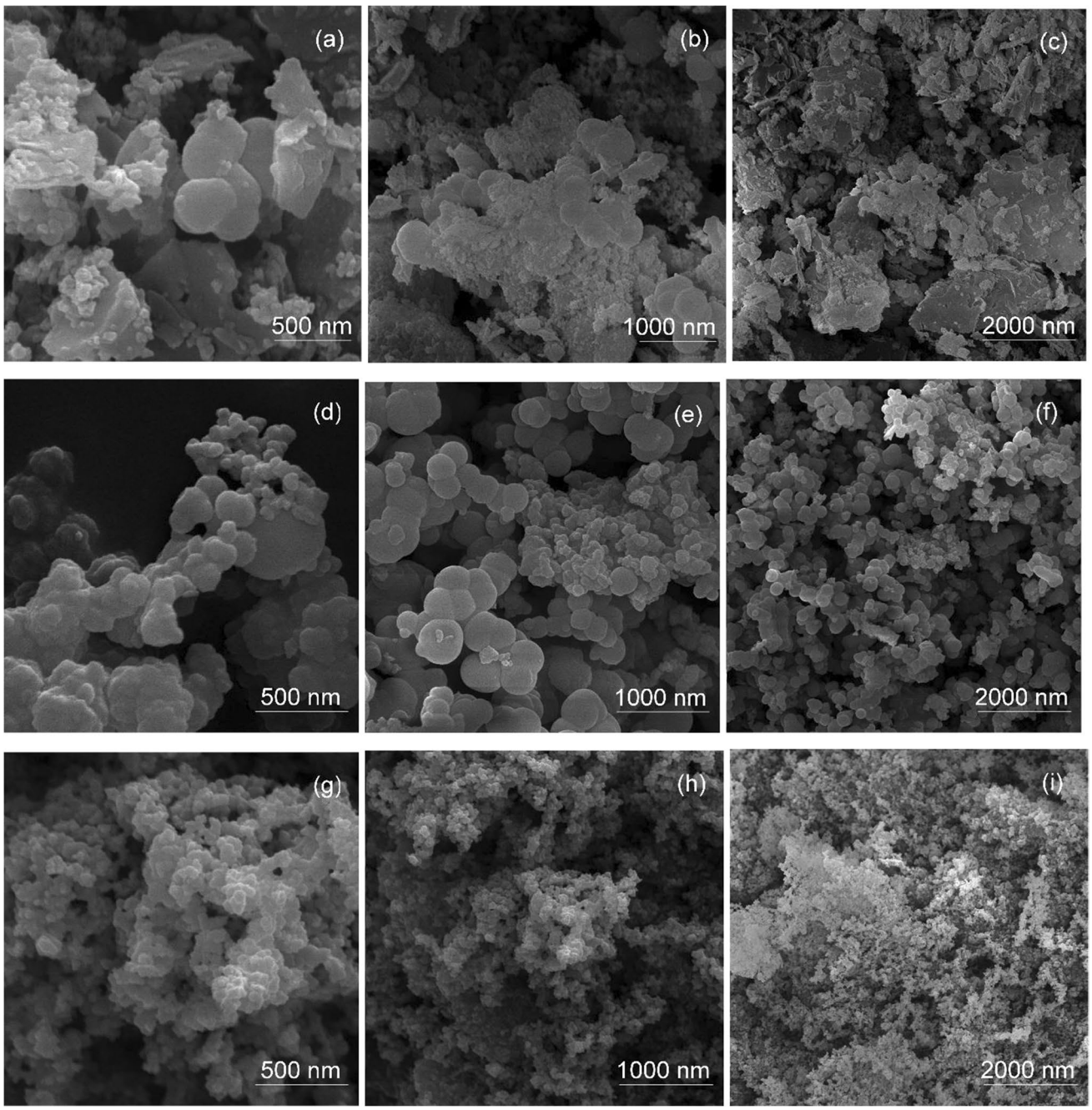

Fig. 2 SEM images of samples Si_{Slag} (**a**–**c**), Si_{MS} (**d**–**f**) and A-60 (**g**–**i**)

(Fig. 2d–f), the formation of spherical particles is observed, which coalesce during the synthesis and thus the formation of sufficiently large particles occurs. These large coalesced particles form loose aggregates and agglomerates with a characteristic fractal structure. The grainy silica structures can be seen for A-60 sample, synthesized by pyrogenic method (Fig. 2g–i).

3.2 IR Spectroscopy

It is known, that various crystalline and anhydrous modifications of silica (with the exception of stishovite) are inorganic 3D polymers, the structural unit of which is a silicon–oxygen tetrahedron: a silicon atom is located in the center of such a regular tetrahedron, and oxygen atoms serve as vertices. Tetrahedra are interconnected by their vertices, that is, each atom is connected to two *Si* atoms [3, 6]. Amorphous fumed silica is formed by similar tetrahedra, which randomly combine into protoparticles (~ 1 nm in diameter) during synthesis in the flame, which then form primary particles (5–50 nm) and secondary structures (aggregates, agglomerates).

The surface of such silica has a rather complex structure. The presence of randomly placed tetrahedra determines the features of the surface structure and the arrangement of OH groups, the placement of which at different distances from each other complicates the study of the properties of the HDS [1–10].

The IR spectra of all the investigated samples (Fig. 3) demonstrate the presence of characteristic absorption bands of bending vibrations *Si–O-Si* at 468 cm^{-1} (intense) and *O-Si–O* at 800 cm^{-1} (medium intensity), bands of stretching vibrations *Si–O-Si* in the range of 1000–1200 cm^{-1} (Fig. 3a–c). This distinct band characterizes the reactivity of silica. Absorption bands that are related to *OH*-groups are identified as follows: (i) the band centered at 3740–3750 cm^{-1} is ascribed to the *Si–OH* stretching vibration of isolated surface silanols; (ii) band at 3540–3550 cm^{-1} can be assigned to vicinal silanols (*OH⋯OH*, isolated pairs of adjacent OH-groups linked by hydrogen bonds); and (iii) the broad band at 3650–3715 cm^{-1} can be attributed to silanols which are perturbed by interparticle contact and linked with sorbed water molecules by hydrogen bonds [28]. Bands at 1636, 3200–3500 cm^{-1}, related to adsorbed water bonded with silanol groups by hydrogen bonds, indicate its significant content in the Si_{Slag} and Si_{MS} samples, which is associated with the peculiarities of the synthesis conditions. In the insert of Fig. 3d, an absorption band at 3750 cm^{-1} is visible, which corresponds to the main sorption centers – free

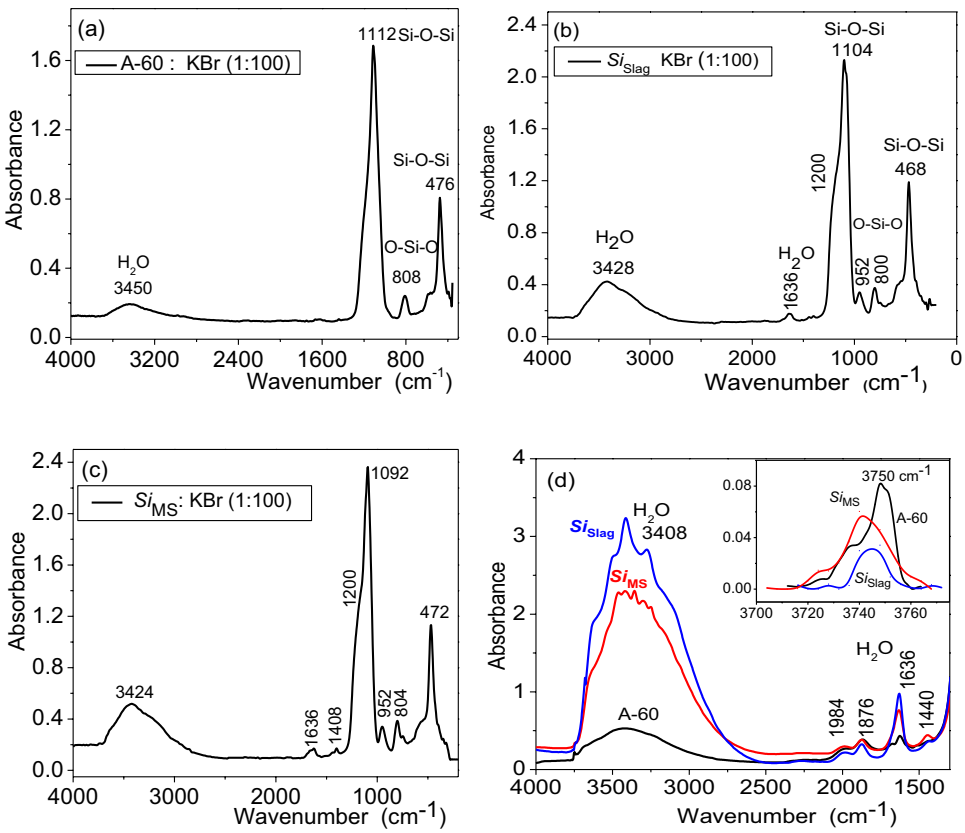

Fig. 3 IR spectra of amorphous silicon dioxides A-60, Si_{Slag}, Si_{MS} samples: **a**–**c**) with KBr in a ratio of 1:100, **d**) without KBr, taken for transmission

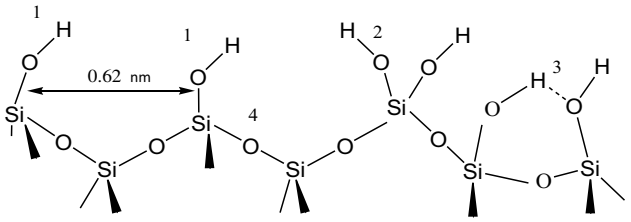

Fig. 4 Schematic illustration of the most common variants of the surface structures of highly dispersed silica [3, 29, 30]

silanol groups ≡*Si–OH*, which are evenly distributed on the silica surface. The intensity of this band is quite low due to the high water content in samples Si_{Slag} and Si_{MS}. A slight increase in the intensity of this important band is possible after additional heating of the samples at a temperature 120–150 °C.

The conditions for the synthesis of highly dispersed silica (high temperature in a hydrogen–oxygen flame, the presence of a large amount of water vapor during cooling) contribute to the formation of particles of a regular spherical shape with a narrow size distribution and the formation of a hydroxyl cover on its surface [20, 29, 30]. Based on the analysis of studies summarized in [3, 29, 30], a fragment of the hydroxylated surface of the HDS can be conventionally represented as a diagram (Fig. 4):

According to this scheme, the surface consists of free isolated (terminal) silanol groups (1), which in the IR spectra correspond to the band at 3750 cm^{-1}; silanediol (geminal) groups (2) – 3750 cm^{-1}, connected by hydrogen bonds of neighboring (vicinal) silanol groups (3), located at a distance of ~ 0.3 nm from each other and which correspond to the band 3550 cm^{-1} and siloxane bridges (4) [2, 4, 6, 31]. For pyrogenic forms of amorphous silica, the overwhelming majority of surface hydroxyl groups are isolated, and the distance between them for pyrogenic HDS calcined at 700–900 K is about 0.62 nm [3, 4, 32–34].

3.3 Thermal Analysis

Thermal analysis is a method for studying chemical and physico-chemical processes occurring in a substance under conditions of a temperature changing [35]. One of its functions is to determine the amount of evaporated structural water and hydroxides in materials. In addition, the method makes it possible to determine the structure of thin water films in the composition of materials. Along with the transformations of matter that occur under the impact of the thermal effect, a change in the mass of the sample is recorded which can be determined by the thermogravimetric method (TG) with great accuracy.

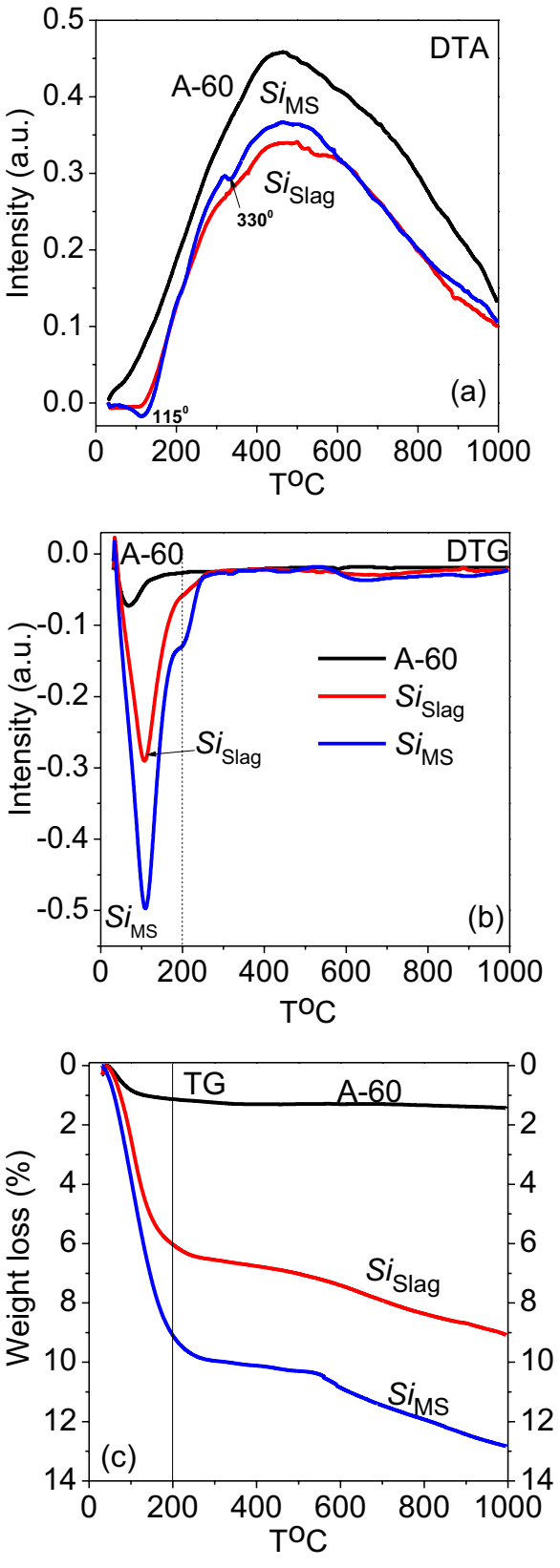

Fig. 5 TG, DTG, and DTA curves of A-60, Si_{Slag} and Si_{MS} amorphous silicon dioxide powders

Figure 5 exhibits the data of thermal analysis of the studied samples of silica A-60, Si_{Slag}; and Si_{MS}. The DTA curves (Fig. 5a) for the A-60 and Si_{Slag} samples do not have any features, but for the Si_{MS}, small peaks are observed in the temperature range of 115 and 330 °C, corresponding to endothermic processes. According to the DTG data (Fig. 5b), when the HDS samples are heated from 0 to 1000 C, one endothermic process is observed with a maximum at 100 °C, which indicates the removal of physically adsorbed water, and stops before 200 °C. Sample Si_{MS} has the highest intensity of this peak, while A-60 has the lowest intensity. In this case, up to 200 °C, the weight loss is 1.1% for A-60; 6% for Si_{Slag}; and 9% for Si_{MS} (Fig. 5c). With an increase in the heating temperature of silica, silanol groups are able to condense, forming siloxane bonds, and water is removed in the steam form. With a gradual increase in the heating temperature to 1000 °C, a further decrease in the mass of samples Si_{Slag} and Si_{MS} is observed, which is probably associated with the process of dehydroxylation of the surface of the SiO_2 samples, since there are several types of OH-groups on the silica surface (single, vicinal and geminal OH-groups, hydrogen bonded and free) [24, 25]. The mass loss for silica samples after complete cooling of the furnace was: A-60 – 1.6%, Si_{Slag} – 9.2%, Si_{MS} – 13.0% (Fig. 5c).

It is known that the content of different forms of water adsorbed on the surface of dispersed or porous oxides depends on the surface nature, preparation temperature and can vary in wide range: from almost zero (heated samples retaining mostly single hydroxyl groups *Si–OH*) to ten or more percent, when most of the water adsorbed on the surface is in molecular form. Adsorption and desorption of water from the pyrogenic oxides surface depends on the concentration and types of surface hydroxyl groups, specific surface area and type of packaging of primary particles in oxide aggregates. Almost all properties of dispersed oxides depend on the content and type of surface *OH* groups [13, 22–24], which contribution to the total TPD spectrum of desorbed water depends on the concentration of these groups and their location on the surface and texture characteristics of the material.

The mass spectra of the products of thermoprogrammed desorption from the surface of the synthesized SiO_2 samples at two temperatures (T = 27 °C and T = 600 °C) are shown in Fig. 6a, c, e. Interpretation of the most intense signals in mass spectra indicates that the most probable volatile products are *m/z* 2 (H_2), *m/z* 16 (*O*), *m/z* 17 (*OH*), *m/z* 18 (H_2O), *m/z* 28 (*CO*), *m/z* 44 (CO_2), *m/z* 44 (NO_2). Analysis of TPD mass spectra demonstrates that the main the lines of *m/z* 2 (H_2) and *m/z* 44 (CO_2) are at low temperatures. At high temperatures, the lines of *m/z* = 17, 18 indicate that hydroxyl radicals *OH* and water molecules H_2O are the main product of TPD.

According to the analysis of the thermograms of the main products (Fig. 6b, d, f) desorbed from the surface of the SiO_2 samples, the desorption process occurs in two or three stages. Molecular hydrogen is desorbed in three stages at temperatures of 95 °C, 170–185 °C, and 570–600 °C, apparently because of the type of bonds with the surface (low-temperature hydrogen can be responsible for Van der Waals' forces and chemisorption, and high-temperature hydrogen – for diffusion from the volume. For curves of oxygen and hydroxyl radical, only two desorption stages are observed. The H_2O desorption curve as the main component confirms the presence of a large amount of adsorbed water in the samples (Fig. 6). The H_2O desorption process occurs in three stages at different temperature maxima: at $T_{max} = 95$ and $T_{max} = 185$ °C adsorbed water is released, the release area 250 °C—600 °C is probably associated with the process of dehydroxylation of the surface of the SiO_2 samples, since there are several types of OH groups on the silica surface (single, vicinal and geminal OH groups, hydrogen bonded and free) [24, 25]. The desorption stage at $T_{max} = 185$ °C (Fig. 6b) presumably is related to the products of *CO* and CO_2. The wide maximum for *m/z* 44 can be responsible for both *COOH* and NO_2. this may be due to the fragmentation of hydrocarbons under the action of an electron beam used as an ionization source.

The thermogram of water desorption for a sample of pyrogenic silica A-60 obtained in a vacuum of ~ 10^{-5} Pa (Fig. 6b) indicates that the amount of molecularly adsorbed water (peaks at 125 and 286 °C), which remains after degassing at room temperature, is two times higher compared to the associative desorbed water (peak at 560 °C), but this amount is generally an order of magnitude lower than the water amount in the samples obtained by the fluoride method of synthesis Si_{slag} and Si_{MS}. This is due to the features of each synthesis method.

Several factors affect the distribution functions of the activation energy of water desorption: (i) different content of terminal and bridged hydroxyl groups for different samples (as sources of associatively desorbed water molecules); (ii) differences in the surface topology (i.e., in the distribution of distances between neighboring groups and the resulting stresses during the associative desorption of water) and the morphology of primary and secondary particles (which affects the adsorption potential for molecularly adsorbed water, its amount and the desorption rate and interparticle mass transfer); (iii) differences in S_{BET} values (i.e., in the adsorption amount per gram of adsorbent) and (iv) different amount of adsorbed water (due to all of the above factors), which also depends on the sample temperature [13, 23, 24].

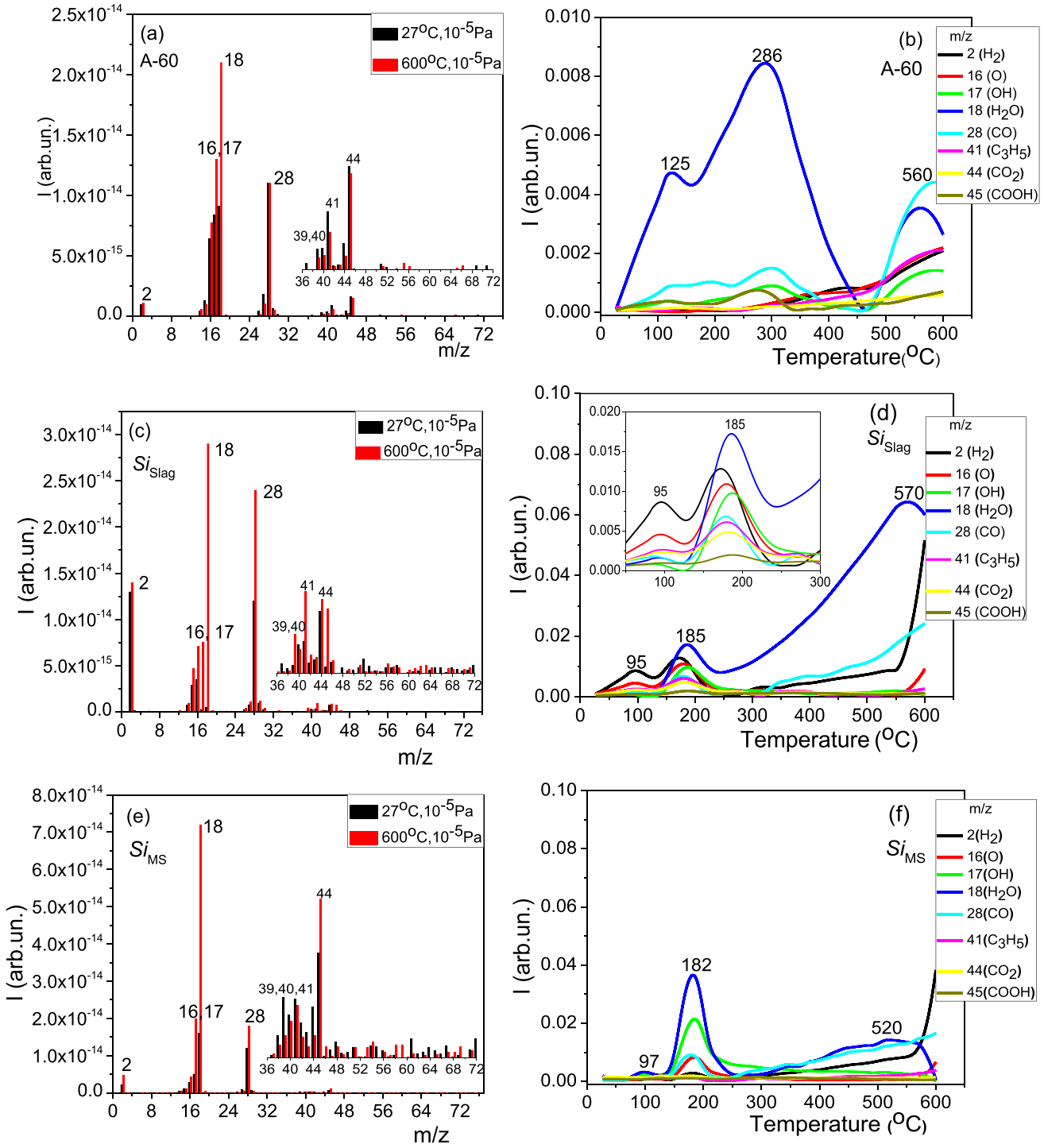

Fig. 6 TPD mass spectrum obtained during the SiO_2 samples thermolysis at T = 27 and 600 °C (**a**, **c**, **e**) and thermograms of the main desorption products H_2 (*m/z* 2), O (*m/z* 16), OH (*m/z* 17), H_2O (*m/z* 18), CO (*m/z* 28), CO_2 (*m/z* 44), NO_2 (*m/z* 44) (**b**, **d**, **f**)

As seen from Fig. 7a, the distribution function of the activation energy of water desorption (mass 18) from the surface of the A-60 silica sample demonstrates the presence of weakly bound water, which corresponds to *peaks 1* and *2* at 70 and 108 kJ/mol, as well as *peak 3*, characteristic of strongly bound water in the region of 160 kJ/mol. The intensity of this peak is two times lower than *peak 2*, which may be due to the significantly lower amount of strongly bound water

in this silica sample. But these value of activation energies are an order of magnitude lower than ones for silica samples obtained by the fluoride synthesis method (Fig. 7b, c).

The activation energy obtained from TPD data is 60–80 kJ/mol during water desorption from the surface of samples Si_{Slag} and Si_{MS}, which corresponds to *peak 1* of the $f(E_a)$ function, as well as *peak 2* with a maximum of 100 kJ/mol at 180 °C and refers to the desorption of molecularly adsorbed water (Fig. 7b, c). Moreover, for sample Si_{MS}, *peak 2* has a two times greater intensity than for Si_{Slag}, which indicates a significant amount of water in this sample, which remains after degassing at room temperature [23].

The position of *peaks 3* of the function $f(E_a)$ for samples Si_{Slag} and Si_{MS} at 160–180 kJ/mol is due to the associatively desorbed water at 400–600 °C (Fig. 7b, c). For sample Si_{Slag}, this peak has three times higher intensity as for Si_{Slag}. This may be due to both the structure of the aggregates, the features of the hydroxyl cover, and the localization of water molecules, which, in turn, can form clusters and domains, as well as be localized in the interparticle gaps and pores.

3.4 Thermal Effect of Immersion

The heats of immersion of highly dispersed silicas Si_{Slag}, Si_{MS} and fumed silica A-60 in polar (water) and non-polar (*n*-decane) liquids have been studied. For the study, the samples were preliminarily degassed and heated to remove physically adsorbed water from their surface.

Wetting is a process in which a decrease in free energy occurs in a system of three phases in contact. Therefore, heat is released during the wetting process. The heat of immersion can serve as a characteristic of the liquid ability to wet a solid.

The decrease in the free energy of the system upon wetting depends both on the surface area and the surface nature. The hydrophilicity index (K_h) eliminates the surface area factor, since the surface area remains constant when wetted with both water and *n*-decane. Thus, the hydrophilicity index is a convenient characteristic for assessing the influence of the surface nature on the interaction with polar or non-polar liquids.

The thermal effect of immersion according to the Gibbs–Helmholtz equation is

$$q = \sigma - T\frac{d\sigma}{dT}, \tag{8}$$

where q – thermal effect of immersion, σ – surface energy, T – temperature.

It follows that the thermal effect depends on the temperature.

At the end of the formation of the first layer of adsorbed water, 55–70% of heat from the total amount is released.

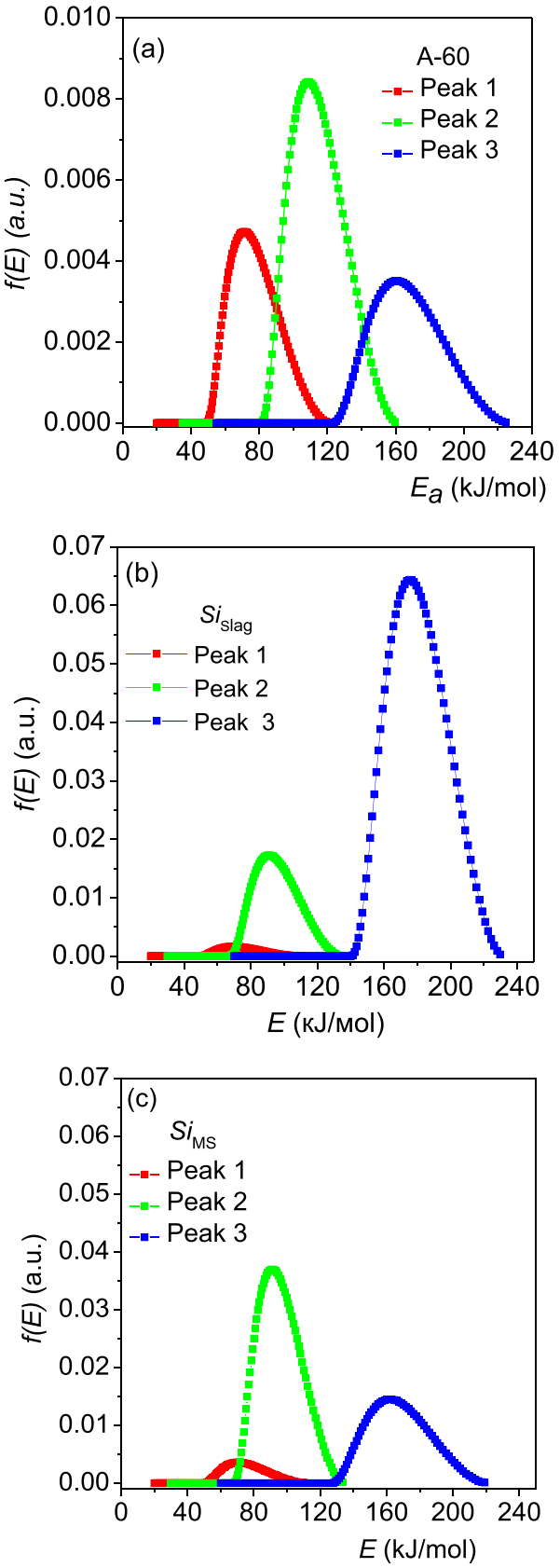

Fig. 7 Distribution function of the activation energy of water desorption (mass 18) from the surface of silica samples A-60, Si_{Slag} and Si_{MS}

Eiler in his review noted the dependence of the heat of immersion on the surface hydration degree [4]. Thus, according to his data, at a maximum degree of hydroxylation of 4.7 OH groups/nm^2, the heat of immersion can approach a value of 200 mJ/m^2. The unwettability or hydrophobic nature that the siloxane surface exhibits during its contact with water allowed Laskowsky and Kitcher [4] to conclude that the work of the adhesive forces of water in contact with a solid surface consists of three components: i) dispersion forces (Van der Waals' forces); ii) hydration of non-ionic polar centers (i.e. binding of water molecules to *Si–OH* groups) and iii) dissociation.

Figure 8 shows the calorimetric curves of immersion in water and *n*-decane of silica samples obtained using various synthesis methods, calculated per 1 g of the initial sample and 1 m^2 of its surface. From the data obtained, it can be concluded that all the systems under study are hydrophilic, that is, the hydrophilicity index for all the studied samples is greater than one.

Moreover, according to the heat of immersion in water (Q_w) normalized per 1 m^2 of surface and K_h values, the hydrophilicity of the studied samples Si_{Slag} and Si_{MS} is significantly higher than the hydrophilicity of fumed silica A-60, which may be due to a higher concentration of surface silanol groups and water molecules adsorbed on the surface of the samples silica Si_{Slag} and Si_{MS}, and is explained by the peculiarities of their synthesis. The hydrophilicity indexes of samples Si_{Slag} and Si_{MS} are 10 and 20, respectively, which is significantly higher than for pyrogenic silica A-60, for which $K_h = 2$ (Table 3).

4 Conclusions

Thus, silica samples Si_{Slag} and Si_{MS} synthesized by the fluoride method have a developed hydroxyl cover and contain various forms of adsorbed water on their surface, which is removed at different temperatures in several stages. This is confirmed by the methods of IR, derivatography and TPDMS. In addition, sample Si_{MS} contains greater amount of water than sample Si_{Slag}. This may be due to the presence of several layers of adsorbed water on its surface. At the same time, the heat of immersion in water (as a polar liquid), calculated per m^2 of its surface, is higher than for A-60 and Si_{Slag}. The hydrophilicity indexes of samples Si_{Slag} and Si_{MS} are 10 and 20, respectively, which is significantly higher than for pyrogenic silica A-60, for which $K_h = 2$.

According to nitrogen adsorption–desorption data, the Si_{Slag} sample has a developed surface area $S_{BET} = 64$ m^2/g, which is close to that of A-60 silica obtained by the pyrogenic synthesis method ($S_{BET} = 80$ m^2/g) and is predominantly

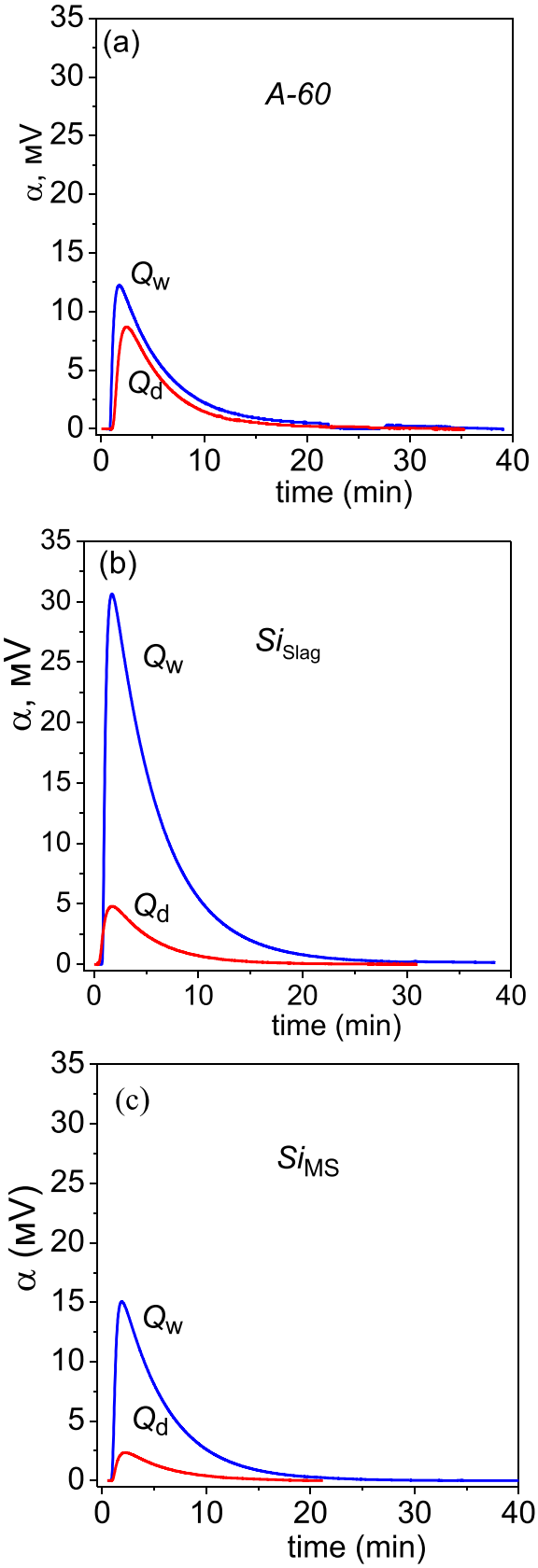

Fig. 8 Calorimetric curves of immersion in water and *n*-decane for silica samples: A-60, Si_{Slag} and Si_{MS} ($m_{SiO_2} = 100$ mg)

Table 3 Heats of immersion in water and *n*-decane for silica samples obtained by different synthesis methods

Sample	S, m^2/g	Q_w		Q_d		K_h
		J/g	J/m^2	*J/g*	J/m^2	
A-60	80	11.17	0.14	6.2	0.078	2
Si_{Slag}	64	42.91	0.68	4.39	0.069	10
Si_{MS}	11	24.27	1.75	1.15	0.083	20

mesoporous ($S_{meso}=55$ m^2/g with $R_{p,V}=7.6$ nm). At the same time, the Si_{MS} sample synthesized from microsilica by the same fluoride synthesis method has a significantly lower specific surface ($S_{BET}=11$ m^2/g), and does not have micro and mesoporosity. Such significant differences between silica samples obtained by the fluoride synthesis method are associated with the use of different raw materials.

Acknowledgements The authors are grateful to Professor V.M. Gun'ko for the developed and provided program for calculating the pore size distribution and distribution function of activation energy of water desorption.

Authors Contributions All authors contributed to the study conception and design.

Mirtemir Sh. Kurbanov: Conceptualization, Methodology;

Sardor A. Tulaganov: Investigation; Visualization;

Lyudmila S. Andriyko: Investigation, Analysis, Interpretation, Writing-Reviewing and Editing;

Olena V. Goncharuk: Investigation; Writing-Original draft preparation;

Natalia V. Guzenko: Investigation, Validation;

Yurii M. Nychyporuk: Investigation, Formal analysis.

Andrii Marynin: SEM investigation and analysis.

The first draft of the manuscript was written be Lyudmila Andriyko and all authors commented on previous versions of the manuscript. All authors read and approved the final manuscript.

Funding This work was supported by the Ministry of Innovative Development of the Republic of Uzbekistan grant No FZ-201907045.

Data Availability All data obtained or analysed during this study are included in this published article.

Declarations

Ethical Responsibilities of Authors The manuscript is original and is not submitted to another journal. The article has not been published previously. The manuscript has been written by the stated authors who are ALL aware of its content and approve its submission. The article is not under consideration for publication elsewhere. No conflict of interest exists. If accepted, the article will not be published elsewhere in the same form, in any language, without the written consent of the publisher.

Consent to Participate All authors, whose names are listed in the manuscript, confirm their participation in the study and made their significant contribution.

Consent for Publication All authors have approved the last version of manuscript for submission and give their consent to the publication of the data presented in the article. All authors are responsible for the accuracy of the presented data.

Competing Interests The authors declare that they have no competing interests.

Financial Interests Authors declare they have no financial interests.

References

1. Chuiko AA (2003) Medical chemistry and clinical applications of silicon dioxide. Naukova dumka, Kiev (in Russian)
2. Chuiko AA (2001) Chemistry of Silica Surface. UkrINTEI, Kiev (in Russian)
3. Legrand AP (1998) The Surface Properties of Silicas. Wiley, New York
4. Iler RK (1979) The Chemistry of Silica. Wiley, Chichester
5. Blitz JP, Gun'ko, (2006) Surface chemistry in biomedical and environmental science, NATO science series II: Mathematics, physics and chemistry, vol 228. Springer, Dordrecht. https://doi.org/10.1007/1-4020-4741-X
6. Hubbard AT (2002) Encyclopedia of surface and colloid science. Marcel Dekker, New York
7. Bergna HE, Roberts WO (2006) Colloidal Silica: Fundamentals and Applications. CRC Press, Boca Raton. https://doi.org/10.1201/9781420028706
8. Shpak AP, Gorbik PP (2009) Nanomaterials and supramolecular structures. Springer. https://doi.org/10.1007/978-90-481-2309-4
9. Basic characteristics of aerosil fumed silica, 4th edn. Tech. Bull. Fine Particles 11; Evonik Industries: Hanau, 2014. Aerosil®–Fumed Silica. Technical Overview; Evonik Industries: Hanau. 2015. http://www.aerosil.com/product/aerosil/en/products/hydrophobic-fumed-silica/Pages/default.aspx. Accessed 1 March 2019
10. Davraz M, Gunduz L (2005) Engineering properties of amorphous silica as a new natural pozzolan for use in concrete. Cem Concr Res 35(7):125–1261. https://doi.org/10.1016/j.cemconres.2004.11.016
11. Camacho NC, Vega Baudrit JR, Urena YC (2018) Basis and Applications of Silicon Reinforced Adhesives. Organ Med Chem IJ 5(1):18–29. https://doi.org/10.19080/OMCIJ.2018.05.555654
12. Linec M, Music B (2019) The effects of silica-based fillers on the properties of epoxy molding compounds. Materials 12(11):1811. https://doi.org/10.3390/ma12111811
13. Gun'ko VM, Mironyuk IF, Zarko VI, Voronin EF, Turov VV, Pakhlov EM, Goncharuk EV, Nychiporuk YM, Vlasova NN, Gorbik PP, Mishchuk OA, Chuiko AA, Kulik TV, Palyanytsya BB, Pakhovchishin SV, Skubiszewska-Zięba J, Janusz W, Turov AV, Leboda R (2005) Morphology and surface properties of fumed silicas. J Colloid Int Sci 289(2):427–445. https://doi.org/10.1016/j.jcis.2005.05.051
14. Gao G-M, Zou H-F, Gan S-C, Liu Z-J, An B-C, Xu J-J, Li G-H (2009) Preparation and properties of silica nanoparticles from oil shale ash. Powder Technol 191(1–2):47–51. https://doi.org/10.1016/j.powtec.2008.09.006
15. Ai Ch, Xiao Y, Wen W, Yuan L (2011) Large scale and environmentally friendly preparation of micro-submicron spherical

silica and their surface effect in resin materials. Powder Technol 210(3):323–327. https://doi.org/10.1016/j.powtec.2011.04.003
16. Kurbanov MSh, Abdurakhmanov BM, Ashurov HB (2018) Prospects for the Production of Silicon and Solar Energy Products in the Republic of Uzbekistan. Appl Solar Energy 54(2):85–90. https://doi.org/10.3103/S0003701X1802007X
17. Abdurakhmanov BM, Ashurov HB, Kurbanov MSh, Nuraliev UM (2014) Modernization of the Technology for Obtaining Technical Silicon for Solar Energy. Appl Solar Energy 50(4):282–286. https://doi.org/10.3103/S0003701X14040045
18. Abdurakhmanov BM, Kurbanov MSh, Tulaganov SA, Ernazarov M, Andriyko LS, Marinin AI, Shevchenko AY (2021) Synthesis of highly dispersed amorphous silicon dioxide powders from industrial metallurgical waste. Uzbek Phys J 23(1):65–74 https://doi.org/10.52304/.v23i1.226 (in Russian)
19. Kurbanov MSh, Tulaganov SA, Ernazarov M, Andriyko LS, Marinin AI, Shevchenko AYu (2021) Properties of Amorphous Silica Synthesized from Copper-Smelting Slags. J Nano Electron Phys 13(6):06024(5pp). https://doi.org/10.21272/jnep.13(6).06024
20. Gregg SJ, Sing KSW (1982) Adsorption, Surface Area and Porosity. Academic Press, London. https://doi.org/10.1002/bbpc.19820861019
21. Adamson AW, Gast AP (1997) Physical Chemistry of Surface, 6th edn. New York, Wiley. https://doi.org/10.1126/science.160.3824.179
22. Gun'ko VM (2014) Composite materials: textural characteristics. Appl Surf Sci 307:444–454. https://doi.org/10.1016/j.apsusc.2014.04.055
23. Gun'ko VM, Zarko VI, Chuikov BA, Dudnik VV, Ptushinskii YuG, Voronin EF, Pakhlov EM, Chuiko AA (1998) Temperature-programmed desorption of water from fumed silica, titania, silica/titania, and silica/alumina. Int J Mass Spectrom Ion Process 172(161):161–179. https://doi.org/10.1016/S0168-1176(97)00269-3
24. Gun'ko VM, Turov VV, Gorbik PP (2009) Water at the interface. Naukova dumka, Kiev (in Russian)
25. Gunko V, Zarko V, Turov V, Oranska O, Goncharuk E, Nychiporuk Y, Pakhlov E, Yurchenko G, Leboda R, Skubiszewska-Zieba J, Osovskii V, Ptushinskii Y, Derzhypolskyi A, Melenevsky D, Blitze J (2009) Morphological and structural features of individual and composite nanooxides with alumina, silica, and titania in powders and aqueous suspensions. Powder Technol 195(3):245–258. https://doi.org/10.1016/j.powtec.2009.06.005
26. Goncharuk OV (2015) The heat of immersion of modified silica in polar and nonpolar liquids. J Therm Anal Calorim 120:1365–1373. https://doi.org/10.1007/s10973-015-4438-y
27. Gun'ko VM, Turov VV, Zarko VI, Goncharuk OV, Pakhlov EM, Skubiszewska-Zięba J, Blitz JP (2016) Interfacial phenomena at a surface of individual and complex fumed nanooxides. Adv Colloid Interf Sci 35:108–189. https://doi.org/10.1016/j.cis.2016.06.003
28. Gun VM, Pakhlov EM, Skubiszewska-Zięba J, Blitz JP (2017) Infrared spectroscopy as a tool for textural and structural characterization of individual and complex fumed oxides. Vib Spectrosc 88:56–6. https://doi.org/10.1016/j.vibspec.2016.11.003
29. Gun VM, Mironyuk IF, Zarko VI, Turov VV, Voronin EF, Pakhlov EM, Goncharuk EV, Leboda R, Skubiszewska-Zieba J, Janusz W, Chibowski S, Levchuk YuN, Klyueva AV (2001) Fumed silicas possessing different morphology and hydrophilicity. J Colloid Int Sci 242(1):90–103. https://doi.org/10.1006/jcis.2001.7736
30. Gunko VM (2000) Influence of the nature and state of the surface of highly dispersed oxides of silicon, aluminum and titanium on their sorption properties. Theoret Exp Chem 36(1):1–29 (in Russian)
31. Kiselev AV, Lygin VI (1972) Infrared spectra of surface compounds. Nauka, Moscow (in Russian)
32. Zuravlev LT (1987) Concentration of Hydroxyl Groups on the Surface of Amorphous Silicas. Langmiur 3:316–318. https://doi.org/10.1021/la00075a004
33. Zhuravlev LT (2000) The surface chemistry of amorphous silica. The Zhuravlev model. J Colloid Surf A 173:1–38. https://doi.org/10.1016/S0927-7757(00)00556-2
34. Khouchaf L, Boulahya K, Das PP, Nicolopoulos S, Kis VK, Lábár JL (2020) Study of the Microstructure of Amorphous Silica Nanostructures Using High-Resolution Electron Microscopy, Electron Energy Loss Spectroscopy, X-ray Powder Diffraction, and Electron Pair Distribution Function. Materials 13(19):4393. https://doi.org/10.3390/ma13194393
35. Almyashev VI, Gusarov VV (1999) Thermal methods of analysis. Tutorial. St. Petersburg (in Russian)